

# Geophysical Research Letters



## RESEARCH LETTER

10.1029/2019GL081939

### Key Points:

- East Asian Monsoon variability is impacted by ENSO
- Summer and winter EAM variability increased during the LIA
- Asian continental temperature is not the main driver of the EAM

### Supporting Information:

- Supporting Information S1

### Correspondence to:

N. F. Goodkin,  
[ngoodkin@amnh.org](mailto:ngoodkin@amnh.org)

### Citation:

Goodkin, N. F., Bolton, A., Hughen, K. A., Karnauskas, K. B., Griffin, S., Phan, K. H., et al. (2019). East Asian Monsoon variability since the sixteenth century. *Geophysical Research Letters*, 46, 4790–4798. <https://doi.org/10.1029/2019GL081939>





Received 7 JAN 2019

Accepted 11 APR 2019

Accepted article online 16 APR 2019

Published online 2 MAY 2019

## East Asian Monsoon Variability Since the Sixteenth Century

N. F. Goodkin<sup>1,2,3</sup> , A. Bolton<sup>1,4</sup>, K. A. Hughen<sup>5</sup> , K. B. Karnauskas<sup>6,7</sup> , S. Griffin<sup>8</sup>, K. H. Phan<sup>9</sup>, S. T. Vo<sup>9</sup>, M. R. Ong<sup>2</sup>, and E. R. M. Druffel<sup>8</sup> 

<sup>1</sup>Earth Observatory of Singapore, Singapore, <sup>2</sup>Asian School of the Environment, Nanyang Technological University, Singapore, <sup>3</sup>Division of Physical Sciences, American Museum of Natural History, New York, NY, USA, <sup>4</sup>Now at Institute of Environmental Science and Research Ltd., Wellington, New Zealand, <sup>5</sup>Marine Chemistry and Geochemistry, Woods Hole Oceanographic Institution, Woods Hole, MA, USA, <sup>6</sup>Cooperative Institute for Research in Environmental Sciences, Boulder, CO, USA, <sup>7</sup>Department of Atmospheric and Oceanic Sciences, University of Colorado Boulder, Boulder, CO, USA, <sup>8</sup>Earth System Science, University of California, Irvine, CA, USA, <sup>9</sup>Nha Trang Institute of Oceanography, Vietnam Academy of Science and Technology, Hanoi, Vietnam

**Abstract** The East Asian Monsoon (EAM) impacts storms, freshwater availability, wind energy production, coal consumption, and subsequent air quality for billions of people across Asia. Despite its importance, the EAM's long-term behavior is poorly understood. Here we present an annually resolved record of EAM variance from 1584 to 1950 based on radiocarbon content in a coral from the coast of Vietnam. The coral record reveals previously undocumented centennial scale changes in EAM variance during both the summer and winter seasons, with an overall decline from 1600 to the present. Such long-term variations in monsoon variance appear to reflect independent seasonal mechanisms that are a combination of changes in continental temperature, the strength of the Siberian High, and El Niño–Southern Oscillation behavior. We conclude that the EAM is an important conduit for propagating climate signals from the tropics to higher latitudes.

**Plain Language Summary** The monsoon systems across Asia are critical to the many Asian communities for which they supply freshwater and control winter severity. Even small changes in the amount of summer precipitation or strength of winter storms can have devastating effects. Our instrumental records of the monsoons are limited, and therefore so is our understanding of their behavior. Here, we use relative amounts of radiocarbon to reconstruct both the summer and winter East Asian Monsoon from 1584 to 1950. We find that there is significant variability in the monsoon system that appears to be influenced by both tropical and high-latitude climate systems, including a long-term decline in monsoon variability and an inverse relationship between the winter monsoon and the Siberian High at multidecadal frequencies. Both the summer and winter monsoon records indicate that the monsoon system may be a path of communication between the tropics and higher latitudes.

## 1. Introduction

East Asia is an important region for studying climate variability due to its high population density and limited instrumental records. The East Asian Monsoon (EAM) is one of the dominant features of the region's climatology, significantly impacting patterns of continental temperature and precipitation (Lau & Li, 1984; Wang et al., 2000). Much like the Indian monsoon, the energy driving the EAM results from the thermal contrast between the Asian landmass and surrounding seas. In winter, the resulting pressure gradients between the Siberian High (SH) and low-pressure systems over the northwestern Pacific Ocean and Indo-Pacific Warm Pool (IPWP) drive northwesterly surface winds along the China coast and across the South China Sea (Chen et al., 2000), forming the East Asian winter monsoon (EAWM; Figure 1a). Across China and Korea, the winter monsoon controls storm tracks and temperatures, which have significant impacts on travel and energy consumption. In summer, a quasi-stationary thermal low over the warmer Asian land mass leads to the East Asian Summer Monsoon (EASM; Figure 1b), which drives winds from the southwest across the South China Sea toward the continent, shifting northward the Intertropical Convergence Zone and subsequent rains over Asia (Yihui & Chan, 2005). Despite the crucial importance to Asian society and ecosystems, annually resolved, multicentury records of EAM variability and its relationships to neighboring regions are rare.

©2019. The Authors.

This is an open access article under the terms of the Creative Commons Attribution-NonCommercial-NoDerivs License, which permits use and distribution in any medium, provided the original work is properly cited, the use is non-commercial and no modifications or adaptations are made.

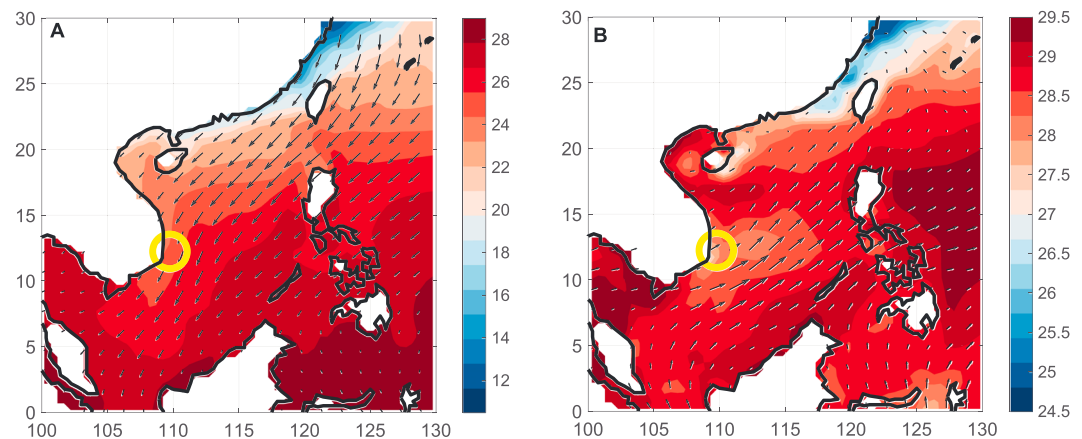


**Figure 1.** Simple Ocean Data Assimilation average SST from 1871 to 1950 (Carton & Giese, 2006). (a) December, January, February average; (b) July, August, September average. The yellow circle indicates the coral site in Vietnam. Arrows indicate wind stress with lengths indicating relative strength. During the winter monsoon, water is driven through the Luzon Strait, delivering higher  $\Delta^{14}\text{C}$  water to Vietnam and south toward the Karimata Strait between Borneo and Sumatra. During the winter monsoon, low-SST, high  $\Delta^{14}\text{C}$  water is advected to the coral site. During the summer monsoon, upwelling delivers lower  $\Delta^{14}\text{C}$  water at the coral site, as seen by suppressed SST originating along the Vietnamese Coast. SST = sea surface temperatures.

On instrumental time scales since 1950, the EAM has been shown to interact with other regional climate phenomena, including the El Niño–Southern Oscillation (ENSO; e.g., D'Arrigo et al., 2005; Xie et al., 2009), Pacific and Indian ocean sea surface temperatures (SST; Li et al., 2010; Wu et al., 2009) and the Arctic Oscillation (AO; Zhao et al., 2018). ENSO, the variation of zonal winds and SST over the tropical Pacific, has a strong but temporally variable relationship with the EAM, where in general, positive ENSO (El Niño) events cool the IPWP and weaken both summer and winter monsoons. ENSO's relationship to the EAM is temporally complex, with atmospheric teleconnections allowing the summer ENSO to influence the winter monsoon and vice versa (Song & Zhou, 2014a, 2014b; Wu et al., 2009; Xie et al., 2009). The Pacific Decadal Oscillation (PDO), defined by the leading empirical orthogonal function of Pacific SSTs north of 20°N after removing global SST (Deser et al., 2010), has been documented to alter the EAM directly and through its response to ENSO. When the PDO is in its high phase, the relationship between ENSO and the EAWM is not present (Wang et al., 2008) and in the summer, increasing tropical SSTs from the PDO weaken the summer monsoon, leading to drought in northern and eastern China (Li et al., 2010; Song et al., 2014). Most studies agree that the influences of the PDO and ENSO on the EAM are often intertwined, involving temporally variable teleconnections (Song & Zhou, 2015). The AO, defined by the leading empirical orthogonal function of winter sea level pressure (SLP) north of 20°N (Thompson & Wallace, 2001), has a stronger relationship to the EAM in winter than in summer, though potential causal relationships are poorly understood. An enhanced polar vortex during a positive AO phase could prevent cold arctic air from traveling south, warming continental Asia and weakening the SH and the subtropical jet, leading to a less active EAWM (He et al., 2017).

During the late twentieth century, the EAM has been weakening, documented in winter by declining moisture and surface winds by as much as 28% between 1970 and 2000 (Hu et al., 2000; Jiang et al., 2010; Peng et al., 2003; Xu et al., 2006) and in summer by weakening winds and accompanying severe droughts in China (Wang, 2001; Yu et al., 2004). However, instrumental, gridded data sets do not extend prior to the mid-1800s, critically limiting our understanding of this important system's long-term behavior (D'Arrigo et al., 2005; Wang, 2001; Wu & Wang, 2002). Paleoclimate records in the region do exist but are heavily biased toward terrestrial sources that record only summer variability (e.g., Liu et al., 2015) and limit our knowledge of the monsoon's manifestation over the ocean, including its interactions with tropical systems in the South China Sea (Song et al., 2012; Yin et al., 2014). A sole marine record from the Paracel Islands used coral  $\delta^{18}\text{O}$  as a proxy for winter wind speed and confirmed a declining trend over the past 180 years as the hemisphere warmed, as well as a shift in direction and magnitude of ENSO-related impacts (Song et al., 2012). Multicentury records are clearly needed to document and evaluate long-term drivers of EAM

variability. Significantly extending the record of the EAM beyond the last two centuries is key to investigating the full range of variability of this important monsoon system, including its low-frequency variability, response to anthropogenic forcing, and relationship to other modes of climate variability.

Coral radiocarbon measurements reflect changes in water mass circulation in the surface ocean, specifically those linked directly to monsoonal surface winds (Bolton et al., 2016). In the winter (November–February), the EAWM drives surface water from the northeastern South China Sea, delivering lower temperature and higher  $\Delta^{14}\text{C}$  water to Vietnam from the Luzon Strait and the northern equatorial Pacific (Figure 1a). During summer (May–October), southwesterly EASM winds drive surface water to the northeast and cause upwelling of deeper cold, low  $\Delta^{14}\text{C}$  water off the coast of southern Vietnam due to offshore Ekman transport (Figure 1b). Low  $\Delta^{14}\text{C}$  values relative to other records in the region, during both thermonuclear bomb testing (>1950) and the prebomb baseline period, as well as seasonally high  $\Delta^{14}\text{C}$  values in the winter, indicate the influence of both summer upwelling and winter advection on  $\Delta^{14}\text{C}$  at this site (Bolton et al., 2016). We therefore use the  $\Delta^{14}\text{C}$  proxy of seawater circulation in this study to reconstruct monsoon variability from 1584 to 1950 and to understand its linkages to other aspects of the climate system.

## 2. Methods

### 2.1. Subsampling and Analysis

A 4.6-m-long *Porites lutea* core was collected live using a hydraulic drill from 2.5 m below the surface in the South China Sea near Hòn Tre Island, Vietnam ( $12^{\circ}12'49.90''\text{N}$ ,  $109^{\circ}18'17.51''\text{E}$ ) in March 2011. Hòn Tre sits on a shallow (100 m deep) coastal shelf, and the coral is located at the northeastern tip of the island, ~13 km from the mainland. The core was sectioned into 1-cm slabs and cleaned ultrasonically. X-radiographs showing one light and one dark band per year were used as a guide to drill annual samples parallel to the growth axis prior to 1950 bomb testing. Age-model error is likely to result from either a year of no growth or so little growth that the banding is not visible. Age model error accumulates in time with larger errors at the beginning of the record ( $\pm 10$  years) and less error toward modern time ( $\pm 1$  year). From 1945 to 1949, six samples per year were drilled to investigate seasonal variability.

Seven to eight milligrams of coral powder were acidified with 85% phosphoric acid for conversion to  $\text{CO}_2$  gas. The gas was converted to graphite on iron powder via zinc reduction (Xu et al., 2007). The graphite  $^{14}\text{C}$  analyses were then conducted using an accelerator mass spectrometer at the Keck Carbon Cycle AMS Laboratory at the University of California, Irvine, using standard techniques (Southon et al., 2004). We report  $\Delta$  values, a term used for  $^{14}\text{C}$  measurements on geochemical samples corrected for fractionation and known age (Stuiver & Polach, 1977). The accelerator mass spectrometer measurements have a 1 sigma uncertainty of  $\pm 1.8\%$  determined by coral standards and duplicate sample measurements. Coral  $\Delta^{14}\text{C}$  is known to reflect  $\Delta^{14}\text{C}$  of dissolved inorganic carbon in seawater, which is influenced by atmospheric exchange of  $\text{CO}_2$  and sea water circulation (Druffel & Suess, 1983).

An EAWM wind intensity index was calculated by D'Arrigo, Wilson, et al. (2005) from Hadley Center global gridded mean SLP data from  $40^{\circ}$  to  $65^{\circ}\text{N}$ , using the formula of Wu & Wang, 2002; Basnett & Parker, 1997; Wu & Wang, 2002). A regional EAWM index was used because the seawater advection signal is seen throughout a large portion of the South China Sea (Figure 1a). For the EASM, a number of published indices match rainfall in specific locations (Li & Zeng, 2002; Wang et al., 2004); however, the  $\Delta^{14}\text{C}$  record during summer relates specifically to wind stress driving upwelling at the coral location. Therefore, we identify the wind stress data nearest to the coral site, rather than a more spatially complicated EASM index. The southwesterly wind stress is calculated from NOAA 20th Century Reanalysis version 2 (20CRv2) wind vector data from  $11^{\circ}$  to  $13^{\circ}\text{N}$  and  $108^{\circ}$  to  $110^{\circ}\text{E}$  (Figure 2b) using simple vector rotation. Both EAM indices commence in 1871, the earliest time of the climate products, and end in 1950 when the coral record ends. Cross-spectral analysis comparing the coral record to the EAWM and summer wind stress indices utilized a multitaper method with adaptive weighting (Huybers & Denton, 2008). The 90% confidence generated using a Gaussian process where the degrees of freedom were calculated based on the number of windows ( $n = 8$ ) is reported (Amos & Koopmans, 1963).

The coral record is filtered using Gaussian band-pass filters at the frequencies relevant to the monsoon indices (described in section 3 below). Records of annual ENSO (Emile-Geay et al., 2013), winter

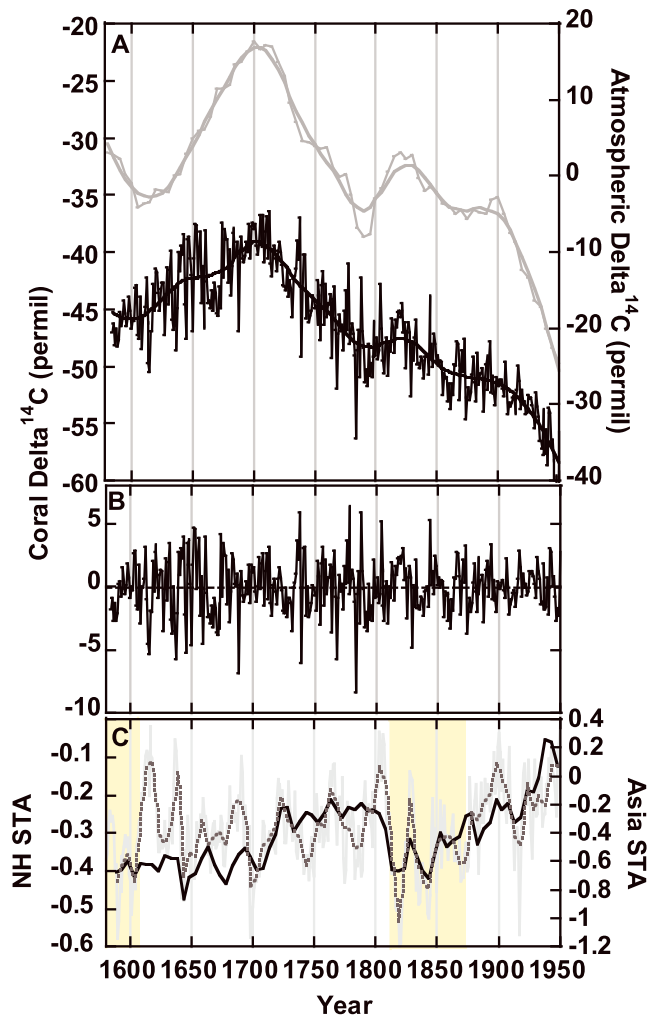


**Figure 2.** Records of  $\Delta^{14}\text{C}$  variability versus time. (a) annual coral  $\Delta^{14}\text{C}$  (black) and 5-year atmospheric  $\Delta^{14}\text{C}$  (gray) both with 100-year smooths (Stuiver & Quay, 1980); (b)  $\Delta^{14}\text{C}_\text{O}$  versus time calculated as the annual coral  $\Delta^{14}\text{C}$  detrended by the coral 100-year smooth with error on an individual measurement shown on the bottom left; (c) Asian summer surface temperature anomalies (Abrams et al., 2016) in annual (gray) and 5-year averages (dashed) and 5-year annual Northern Hemisphere surface temperature anomalies (black; Jones et al., 1998). Shaded areas indicate the cooling periods (1580–1610 and 1810–1870) occurring during the Little Ice Age.

(December–February) SH (D’Arrigo, 2005), and summer Asian surface temperature anomaly (ASTA; Abrams et al., 2016) were similarly filtered, and each record is described in the supporting information. Filtered time series were normalized by subtracting the mean and dividing by the standard deviation of the full record. Fifty-year running variance was calculated using the following formula:

$$\sum \frac{(x-\bar{x})^2}{N-1} \quad (1)$$

where  $x$  denotes an individual climate record value and  $\bar{x}$  is the record’s mean value.  $N$  is the number of years in the variance calculation (50). As the paleo records all indicate age model uncertainty of no more than 10 years at the earliest time of the records, a running variance of 50 years is sufficient to remove concerns of age model error impacting the temporal comparisons.

### 3. Results

Our coral  $\Delta^{14}\text{C}$  record reflects a combination of changes in atmospheric  $^{14}\text{C}$  and local surface water circulation (Figure 2a and supporting information Table S1). The low-frequency (100-year running mean) signal corresponds well with the history of atmospheric  $^{14}\text{C}$  production (Figure 2a), while the high-frequency behavior (<100 years per cycle) is the result of water mass mixing and advection from changes in wind direction and strength. To isolate the variability resulting solely from ocean circulation, we subtracted the  $\Delta^{14}\text{C}$  atmospheric production component (100-year running mean) from the coral  $\Delta^{14}\text{C}$  record to produce  $\Delta^{14}\text{C}_\text{O}$ , a record of circulation-driven  $\Delta^{14}\text{C}$  in the South China Sea (Figure 2b). The record, spanning from 1584 to 1950 CE, extends through a range of temperatures in continental summer Asian and annual Northern Hemisphere reconstructions, including the last cooling periods of the North Atlantic-centered Little Ice Age (1580–1610 CE and 1810–1870 CE; Figure 2c; Abrams et al., 2016; Jones et al., 1998). Subannual samples of  $\Delta^{14}\text{C}$  from 1945 to 1949 CE were used to indicate that bulk annual sampling accurately represents the annual average, and winter maxima and summer minima independently track changes in EAWM and EASM wind stress, respectively (Figure S1). Annual measurements of coral  $\Delta^{14}\text{C}$  can therefore serve as a sensitive proxy for circulation that is mechanistically linked to the strength of both the EAWM and EASM winds off the coast of Vietnam.

The  $\Delta^{14}\text{C}_\text{O}$  record is compared to instrumental records of the EAM, including an EAWM index (D’Arrigo et al., 2005) and EASM summer (July–September) southwesterly wind stress (Li & Zeng, 2002) at the study site (Figures 3a and 3b). The records do not correlate well at annual resolution (Figures 3a and 3b), likely due to the mixed signal of summer and winter  $\Delta^{14}\text{C}$  in each year, as well as influences on ocean circulation not driven by the monsoons. Therefore, we use spectral analysis to identify power and coherence between the coral and monsoon records. Cross-spectral analysis of the  $\Delta^{14}\text{C}_\text{O}$  and EAWM record shows significant (>90%) correlation windows at low and high frequencies, 0.0125 to 0.125 cycles per year (8–80 years) and 0.41 to 0.43 cycles per year (2.3–2.5 years; Figure 3c). Significant correlations between  $\Delta^{14}\text{C}_\text{O}$  and EASM wind stress are found at 0.2 to 0.24 cycles per year (4.2–5 years; Figure 3c). The EAWM and EASM wind stress records also have significant correlations to each other at low frequencies (<0.1 cycles per year; Figure 3d). Previous studies have shown variability in both the EAWM and the SH at 2.4-year periods (D’Arrigo, 2005; Li et al., 2001; Meehl & Arblaster, 2002) as well as multidecadal time scales (Jhun & Lee, 2004; Li et al., 2007; Wang et al., 2009). Similarly, the EASM is directly

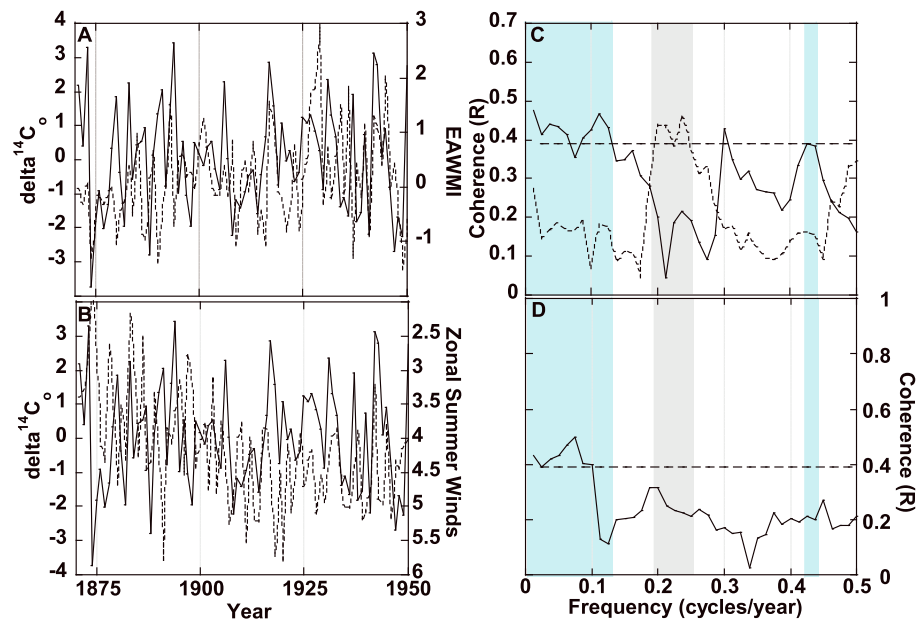


**Figure 3.**  $\Delta^{14}\text{C}_0$  from 1871 to 1950 compared to the EAWM index (D'Arrigo et al., 2005) and to EASM July, August, September wind stress (NOAA 20CRv2) averaged from  $11^\circ$  to  $13^\circ\text{N}$  and  $108^\circ$  to  $110^\circ\text{E}$ . (a) time series for  $\Delta^{14}\text{C}_0$  (solid) and EAWMI (dashed); (b) time series for  $\Delta^{14}\text{C}_0$  (solid) and EASM (dashed); (c) cross-spectral coherence ( $r$ ) plotted versus frequency (cycles per year) for  $\Delta^{14}\text{C}_0$  versus the EAWM index (solid) and EASM wind stress (dashed), 90% confidence shown by hash marks; (d) cross-spectral coherence ( $r$ ) plotted versus frequency (cycles per year) for EAWM versus EASM wind stress (solid), 90% confidence shown by hash marks. Periods when  $\Delta^{14}\text{C}_0$  has significant (90%) coherence to the EAWM and the EASM wind stress are indicated by light blue and gray shading, respectively. The EASM wind stress shows significant coherence to the EAWM, although not to the  $\Delta^{14}\text{C}_0$  (not shown), at multidecadal frequencies. EASM = East Asian Summer Monsoon; EAWM = East Asian winter monsoon.

impacted by ENSO and therefore varies at periods of 4–8 years per cycle (Yihui & Chan, 2005). Spectral power over the full length of the  $\Delta^{14}\text{C}_0$  record shows that four of the six significant power bands occur in these windows of spectral correlation (Figure S2). We, therefore, examine  $\Delta^{14}\text{C}_0$  at these frequencies to investigate monsoon variance.

For the EAWM, the records were band-pass filtered to a frequency of  $0.417\text{ year}^{-1}$  with a width of 0.036 (2.3–2.5 years per cycle) and to a frequency of  $0.0687\text{ year}^{-1}$  with a width 0.1126 (8–80 years per cycle). The two filtered records were then added to generate a record representing the combined EAWM frequencies. The records were also band-pass filtered at a frequency of  $0.22\text{ year}^{-1}$  with a width of 0.04 (4.2–5 years per cycle) to correspond to the EASM southwesterly wind stress. Fifty-year running variances were then calculated for the reconstructed EASM and EAWM  $\Delta^{14}\text{C}_0$  records, the Asian summer surface temperature anomaly, ENSO, and the winter SH records to evaluate changes in behavior over the past several centuries. The records shown in Figure 4 are not indicative of the strength or state of the EAM (positive or negative), but rather demonstrate how variable the systems are through time. A positive correlation in variance indicates that both the climate system and the monsoon were changing significantly (positive and negative), while a negative correlation in variance indicates that either the climate system was variable and the monsoon was invariant, or vice versa.

### 3.1. EASM Variability From 1584 to 1950

At frequencies coherent to the summer wind stress (4.2- to 5-year periods), the EASM  $\Delta^{14}\text{C}_0$  record shows elevated variance around 1650 CE, with a smaller increase at  $\sim 1820$  CE (Figure 4a). Comparing the 50-year running variance of the EASM  $\Delta^{14}\text{C}_0$  record to ASTA variance shows inverse trends from 1600 to 1950 CE (Figure 4b) with an anticorrelation ( $r = -0.62$ ). This result contrasts with the modern relationship between the intensities of the EASM and continental temperature, whereby increased continental temperatures drive a stronger monsoon (e.g., Li & Yang, 2010; Song et al., 2014); that is, given this

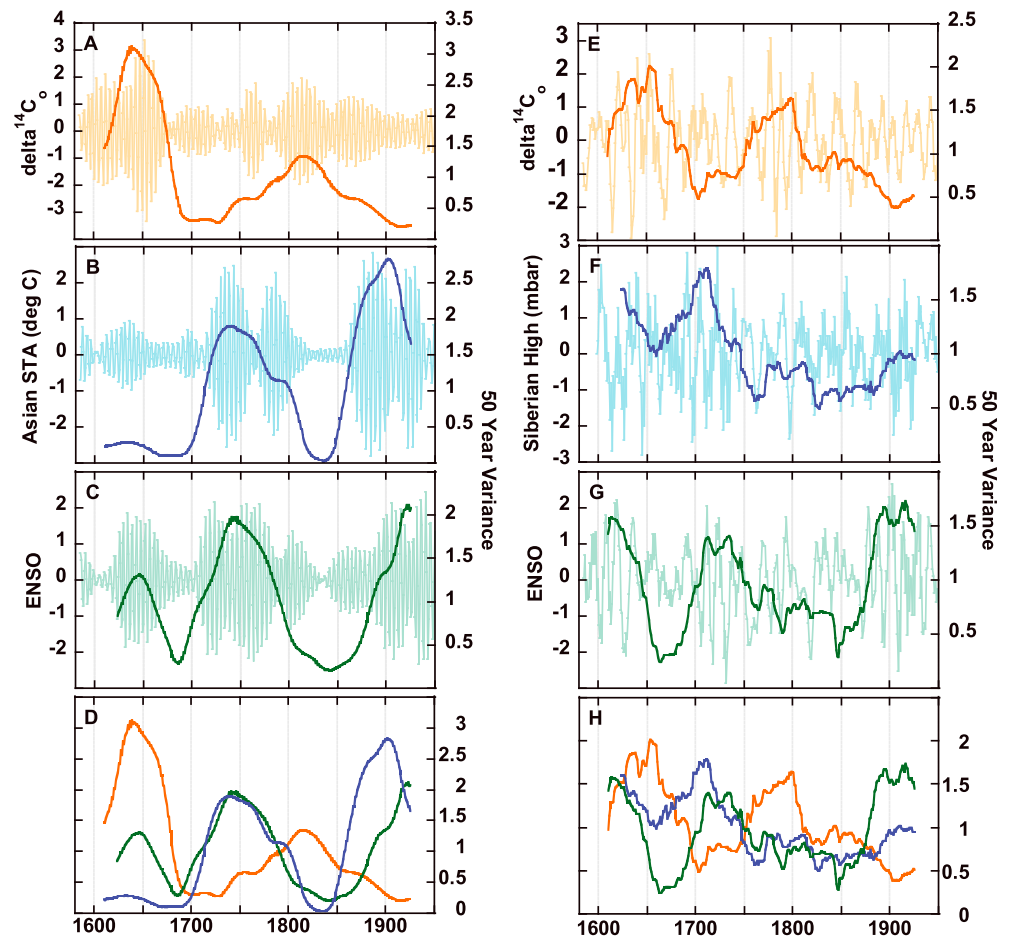


**Figure 4.** Filtered climate records and 50-year running variance versus time. (a)  $\Delta^{14}\text{C}_0$  filtered to frequencies of correlation to EASM summer wind stress (4.2–5 years; light orange) and 50-year running variance of filtered  $\Delta^{14}\text{C}_0$  (orange), (b) summer ASTA filtered to EASM frequencies (4.2–5 years; light blue) and 50-year running variance (dark blue), (c) ENSO filtered (4.2–5 years; light green) and 50-year running variance (dark green), (d) 50-year running variances of filtered records for  $\Delta^{14}\text{C}_0$  EASM (orange), ASTA (blue), and ENSO (green), (e)  $\Delta^{14}\text{C}_0$  filtered to EAWM frequencies (2.3–2.5 and 8–80 years, combined; light orange) and 50-year variance (orange), (f) winter SH filtered (2.3–2.5 and 8–80 years, combined; light blue) and 50-year running variance (dark blue), (g) ENSO filtered (2.3–2.5 and 8–80 years, combined; light green) and 50-year running variance (dark green), and (h) 50-year running variances of filtered records for  $\Delta^{14}\text{C}_0$  EAWM (orange), SH (blue), and ENSO (green). ASTA = Asian surface temperature anomaly; EAWM = East Asian winter monsoon; ENSO = El Niño–Southern Oscillation; SH = Siberian High.

relationship they should experience variability simultaneously. Comparing the variances of the EASM and ASTA to ENSO (filtered at the same frequencies, Figure 4c) shows that changes to ENSO and ASTA variance are in the same direction ( $r = 0.61$ ), but that ENSO variance is weakly anticorrelated to the EASM ( $r = -0.18$ ). The common patterns of variance change are apparent with time, although the magnitudes of variability are not consistent through time (Figure 4d). When ENSO and ASTA variances are high, EASM  $\Delta^{14}\text{C}_0$  variance is low, indicating that the modern continental temperature-EASM and ENSO-EASM relationships are not present, as this would lead to variances increasing and decreasing together (e.g., Li & Yang, 2010; Song et al., 2014).

### 3.2. EAWM Variability From 1584 to 1950

The coral  $\Delta^{14}\text{C}_0$  based EAWM (EAWM  $\Delta^{14}\text{C}_0$ ) record reveals increased variance around 1640–1660 CE and 1750–1800 CE; after these periods the amplitude of variability declines (Figure 4e). Comparing the 50-year running variance of the EAWM  $\Delta^{14}\text{C}_0$  record to a similarly treated winter SH record (D’Arrigo, 2005) shows both to have centennial-scale declining trends ( $-0.0029$  and  $-0.0025$  per year, respectively; Figures 4e and

4f). However, at multidecadal time scales, the running variance records display distinct antiphase variability ( $r = -0.66$ ). Similarly calculated ENSO variance (Figure 4g) positively covaries with the SH at multidecadal scales ( $r = 0.62$ ) but is anticorrelated with the EAWM  $\Delta^{14}\text{C}_\text{O}$  variance ( $r = -0.42$ ; Figure 4h). As above for the EASM  $\Delta^{14}\text{C}_\text{O}$ , the negative correlation between EAWM  $\Delta^{14}\text{C}_\text{O}$  and SH variance on multidecadal time scales is unexpected given modern relationships which imply variance in the SH should drive variance in the EAWM. Similarly, when ENSO variance is low, the SH variance decreases but EAWM variance increases, suggesting a different link between ENSO and EAWM variability than at present (Chen et al., 2000).

#### 4. Discussion

Several mechanisms have been suggested to explain EAM variability, including direct forcing in winter from high-latitude Eurasian surface temperatures (Panagiotopoulos et al., 2005; Takaya & Nakamura, 2013) and the SH driving pressure gradients to lower latitudes, and in summer, by the PDO and changing SSTs altering the land-sea temperature gradient (Song et al., 2014). However, the relationships observed here between both summer and winter monsoon variance and those of high-latitude processes (ASTA and SH) are generally inverse. The net effect in summer is that over the past four centuries variance in ASTA is not driving variance in the EASM, whereas summer ENSO variance appears to strongly dictate not only the EASM variance but also ASTA variance.

For winter, the variance in EAWM  $\Delta^{14}\text{C}_\text{O}$  has a changing connection to SH variance, switching signs between interannual (positive), multidecadal (negative), and centennial (positive) time scales (Figure 4). The positive and negative phases of covariance with the SH suggest a complex interaction of multiple forcing mechanisms influencing EAWM behavior. Modern studies have implicated both the PDO and the winter AO in influencing the global teleconnections driving the EAWM (Ding et al., 2014). However, while no similarly long records of the PDO or winter AO exist, the strong multidecadal relationships between the EAWM, SH, and ENSO variances seen here indicate that EAWM variability may be more strongly tied to the PDO via ENSO than to the SH through the AO. The PDO is believed to override ENSO influence on the EAWM when in a high phase, which could lead to the temporal change in the relationship between the SH and the EAWM (Chen et al., 2000).

The anticorrelated relationship between EAWM  $\Delta^{14}\text{C}_\text{O}$  and SH variance, and the positively correlated relationship between the SH and ENSO variances, indicates that the EAM could serve as a conduit for ENSO modulation of high-latitude climate. As previously mentioned, ENSO is known to impact the EAWM, as related changes to western Pacific SSTs alter South China Sea ocean circulation and land-sea SLP gradients (Chan & Li, 2004; Chang et al., 2004). El Niño events are known to weaken the EAWM (Wang et al., 2000; Zhang et al., 1996) and reduce the frequency of cold surges over China on intraseasonal time scales (Zhang et al., 1997), which may serve to dampen the SH variability. The EAWM itself exerts some influence over climate in the SH region. Strong EAWM circulation causes lower dust concentrations over northern China, with subsequent increased surface temperature from solar radiative forcing (Lou et al., 2017). Similarly, variability attributed to the EAWM resulted in severe snow storms and long-persisting snowpack over northeast Asia during 2007–2008 (Wu et al., 2011), which could also have altered surface temperatures and SLP fields in the region. Thus, the EAWM may be serving as a conduit to propagate low-frequency ENSO signals into the high-latitude SH region. Previous studies confirm decadal-to-centennial-scale changes in the frequency of ENSO events, with significant changes around 1800 CE, including both the latitudinal position of the Intertropical Convergence Zone and the hydrography of the IPWP (Druffel et al., 2015; Newton et al., 2006; Sachs et al., 2009).

In 2008, China experienced winter cooling unmatched in the previous 50 years due to increased EAWM variability. Recent extreme EAWM events suggest that further changes in EAWM variability may continue, shifting to a regime characterized by greater and more frequent extremes and increased variance. Monsoon variance extremes were found in both summer and winter from 1610 to 1680 CE (Figures 4a and 4e). Historical records indicate that during this period the Ming Dynasty in China experienced serious drought beginning in the 1630s, followed by extensive flooding, famine, disease, and ultimately the fall of the Ming Dynasty (Fagan, 2000). The socioeconomic consequences of the 2008 extreme cooling event and other historical events emphasize how we must further improve our understanding of this key monsoon system

for prediction and mitigation of seasonal weather-related impacts. The results presented here strongly motivate both paleoclimate and climate modeling investigations into the dynamics and variability of the relatively understudied EAM, particularly the component of predictability realized through concurrent shifts in the equatorial Pacific Ocean.

### Author Contributions

N. F. G conceived of the project. A. B. subsampled the coral and developed the age model with assistance from M. R. O., E. R. M. D. and S. G. ran the radiocarbon analysis. K. H. P. and S. T. V. identified the coral and conducted field work with N. F. G. and K. A. H. K. B. K. evaluated the coral record relative to the reanalysis data. N. F. G. wrote the manuscript with input from all authors but particularly K. A. H., K. B. K., and E. R. M. D.

### Acknowledgments

Thanks go to G. Williams, W. Tak-Cheung, and J. Ossolinski. Thanks also go to V. Lee, S. H. Ng for coral sampling, and B. Buckley for conversations. This research was supported by the National Research Foundation Singapore NRF Fellowship scheme awarded to N. Goodkin (National Research Fellowship award NRFF-2012-03) and administered by the Earth Observatory of Singapore and the Singapore Ministry of Education under the Research Centers of Excellence initiative. The research was also supported by the Singapore Ministry of Education Academic Research Fund Tier 2 (award MOE2016-T2-1-016). Data are available in Table S1 and the NOAA paleoclimate database.

### References

Abrams, N., McGregor, H. V., Tierney, J. E., Evans, M. N., McKay, N. P., & Kaufman, D. S. (2016). Early onset of industrial-era warming across the oceans and continents. *Nature*, *536*(7617), 411–418. <https://doi.org/10.1038/nature19082>

Amos, D. E., & Koopmans, L. H. (1963). Tables of the distribution coefficient of coherence for stationary bivariate Gaussian processes (No. SCR-483), Sandia National Laboratories (SNL-NM), Albuquerque, NM.

Basnett, T., & Parker, D. (1997). Development of the Global Mean Sea Level Pressure Data Set GMSLP2Rep., Hadley Center for Climate Prediction Research Exeter U. K.

Bolton, A., Goodkin, N. F., Druffel, E. R. M., Griffin, S., & Murty, S. A. (2016). Upwelling of Pacific Intermediate Water in the South China Sea Revealed by Coral Radiocarbon Record. *Radiocarbon*, *58*(1), 37–53.

Carton, J. A., & Giese, B. (2006). SODA: A reanalysis of ocean climate using a Simple Ocean Data Assimilation (SODA). *Monthly Weather Review*, *136*, 2999–3017.

Chan, J. C. L., & Li, C. (2004). The East Asia winter monsoon. In C.-P. Chang (Ed.), *East Asian Monsoon* (pp. 54–106). World Scientific.

Chang, C.-P., Wang, Z., Ju, J., & Li, T. (2004). On the relationship between western Maritime Continent monsoon rainfall and ENSO during northern winter. *Journal of Climate*, *17*, 665–672.

Chen, W., Graf, H. F., & Huang, R. H. (2000). The interannual variability of East Asian winter monsoon and its relation to the summer monsoon. *Advances in Atmospheric Sciences*, *17*(1), 48–60.

D'Arrigo, R. (2005). A reconstructed Siberian High index since A. D. 1599 from Eurasian and North American tree rings. *Geophysical Research Letters*, *32*, L05705. <https://doi.org/10.1029/2004GL022271>

D'Arrigo, R., Wilson, R., Panagiotopoulos, F., & Wu, B. (2005). On the long-term interannual variability of the East Asian winter monsoon. *Geophysical Research Letters*, *32*, L21706. <https://doi.org/10.1029/2005GL023235>

Deser, C., Alexander, M. A., Xie, S.-P., & Phillips, A. S. (2010). Sea surface temperature variability: Patterns and mechanisms. *Annual Review of Marine Science*, *2*(1), 115–143.

Ding, Y., Liu, Y., Liang, S., Ma, X., Zhang, Y., Si, D., et al. (2014). Interdecadal variability of the East Asian winter monsoon and its possible links to global climate change. *Journal of Meteorological Research*, *28*(5), 693–713.

Druffel, E. R. M., Griffin, S., Vetter, D., Dunbar, R. B., & Mucciarone, D. M. (2015). Identification of frequent La Niña events during the early 1800s in the east equatorial Pacific. *Geophysical Research Letters*, *42*, 1512–1519. <https://doi.org/10.1002/2014GL062997>

Druffel, E. R. M., & Suess, H. E. (1983). On the radiocarbon record in banded corals: Exchange parameters and net transport of <sup>14</sup>CO<sub>2</sub> between atmosphere and surface ocean. *Journal of Geophysical Research*, *88*(C2), 1271–1280.

Emile-Geay, J., Cobb, K. M., Mann, M. E., & Wittenberg, A. T. (2013). Estimating Central Equatorial Pacific SST Variability over the Past Millennium. Part II: Reconstructions and Implications. *Journal of Climate*, *26*(7), 2329–2352. <https://doi.org/10.1175/JCLI-D-11-00511.1>

Fagan, B. (2000). *The Little Ice Age: How climate made history 1300–1850*, (p. 246). USA: Basic Books.

He, S., Gao, Y., Li, F., Wang, H., & He, Y. (2017). Impact of Arctic Oscillation on the East Asian climate: A review. *Earth-Science Reviews*, *164*, 48–62.

Hu, Z. Z., Bengtsson, L., & Arpe, K. (2000). Impact of global warming on the Asian winter monsoon in a coupled GCM. *Journal of Geophysical Research*, *105*(D4), 4607–4624.

Huybers, P., & Denton, G. (2008). Antarctic temperature at orbital timescales controlled by local summer duration. *Nature Geoscience*, *1*(11), 787–792.

Jhun, J. G., & Lee, E. J. (2004). A new East Asian winter monsoon index and associated characteristics of the winter monsoon. *Journal of Climate*, *17*(4), 711–726.

Jiang, Y., Luo, Y., Zhao, Z. C., & Tao, S. W. (2010). Changes in wind speed over China during 1956–2004. *Theoretical and Applied Climatology*, *99*(3–4), 421–430.

Jones, P. D., Briffa, K. R., Barnett, T. P., & Tett, S. F. B. (1998). High-resolution palaeoclimatic records for the last millennium: Interpretation, integration and comparison with general circulation model control-run temperatures. *Holocene*, *8*(4), 455–471.

Lau, K. M., & Li, M. T. (1984). The monsoon of East-Asia and its global associations—A survey. *Bulletin of the American Meteorological Society*, *65*(2), 114–125.

Li, C. Y., Sun, S. Q., & Mu, M. Q. (2001). Origin of the TBO-interaction between anomalous East-Asian winter monsoon and ENSO cycle. *Advances in Atmospheric Sciences*, *18*(4), 554–566.

Li, H., Dai, A., Zhou, T., & Lu, J. (2010). Responses of the East Asian summer monsoon to historical SST and atmospheric forcing during 1950–2000. *Climate Dynamics*, *34*, 501–514.

Li, J., & Zeng, Q. (2002). A unified monsoon index. *Geophysical Research Letters*, *29*(8), 1274. <https://doi.org/10.1029/2001GL013874>

Li, Q. P., Ding, Y. H., Dong, W. J., & Yan, G. H. (2007). A numerical study on the winter monsoon and cold surge over East Asia. *Advances in Atmospheric Sciences*, *24*(4), 664–678.



- Li, Y. Q., & Yang, S. (2010). A dynamical index for the East Asian winter monsoon. *Journal of Climate*, 23(15), 4255–4262.
- Liu, J., Chen, J., Zhang, X., Li, Y., Rao, Z., & Chen, F. (2015). Holocene East Asian summer monsoon records in northern China and their inconsistency with Chinese stalagmite  $\delta^{18}\text{O}$  records. *Earth-Science Reviews*, 148, 194–208.
- Lou, S., Russel, L. M., Yang, Y., Liu, Y., Singh, B., & Ghan, S. J. (2017). Impacts of interactive dust and its direct radiative forcing on interannual variations of temperature and precipitation in winter over East Asia. *Journal of Geophysical Research: Atmospheres*, 122, 8761–8780. <https://doi.org/10.1002/2017JD027267>
- Meehl, G. A., & Arblaster, J. M. (2002). The tropospheric biennial oscillation and Asian-Australian monsoon rainfall. *Journal of Climate*, 15, 722–744.
- Newton, A., Thunell, R., & Stott, L. (2006). Climate and hydrographic variability in the Indo-Pacific Warm Pool during the last millennium. *Geophysical Research Letters*, 33, L19710. <https://doi.org/10.1029/2006GL027234>
- Panagiotopoulos, F., Anova, M. S., Hannachi, A., & Stephenson, D. B. (2005). Observed trends and teleconnection of the Siberian High: A recent declining center of action. *Journal of Climate*, 18, 1411–1422.
- Peng, Z. C., He, J. F., Chen, T. G., Nie, B. F., & Liu, G. J. (2003). Sea surface temperature variability in the north side of the South China Sea over the last 55 years revealed by coral delta O-18 records. *Geochimica Et Cosmochimica Acta*, 67(18), A378–A378.
- Sachs, J. P., Sachse, D., Smittenberg, R. H., Zhang, Z., Battisti, D. S., & Golubic, S. (2009). Southward movement of the Pacific intertropical convergence zone AD 1400–1850. *Nature Geoscience*, 2, 519–525.
- Song, F., & Zhou, T. (2014a). The climatology and interannual variability of East Asian summer monsoon in CMIP5 coupled models: Does air-sea coupling improve simulations? *Journal of Climate*, 27, 8761–8777.
- Song, F., & Zhou, T. (2014b). Interannual variability of East Asian summer monsoon simulated by CMIP3 and CMIP5 AGCMs: Skill dependence on Indian Ocean-Western Pacific anticyclone teleconnection. *Journal of Climate*, 27, 1679–1697.
- Song, F., & Zhou, T. (2015). The dominant role of internal variability in modulating the decadal variation of the East Asian summer monsoon-ENSO relationship during the 20th century. *Journal of Climate*, 28, 7093–7107.
- Song, F., Zhou, T., & Qian, Y. (2014). Responses of East Asian summer monsoon to natural and anthropogenic forcings in the 17 latest CMIP5 models. *Geophysical Research Letters*, 41, 596–603. <https://doi.org/10.1002/2013GL058705>
- Song, S. H., Peng, Z. C., Zhou, W. J., Liu, W. G., Liu, Y., & Chen, T. G. (2012). Variation of the winter monsoon in South China Sea over the past 183 years: Evidence from oxygen isotopes in coral. *Global and Planetary Change*, 98–99, 131–138.
- Southon, J., Santos, G., Druffel-Rodriguez, K., Druffel, E., Trumbore, S., Xu, X. M., et al. (2004). The Keck Carbon Cycle AMS laboratory, University of California, Irvine: Initial operation and a background surprise. *Radiocarbon*, 46(1), 41–49.
- Stuiver, M., & Polach, H. A. (1977). Reporting of  $^{14}\text{C}$  data. *Radiocarbon*, 19(3), 355–363.
- Stuiver, M., & Quay, P. D. (1980). Patterns of atmospheric  $^{14}\text{C}$  changes. *Radiocarbon*, 22, 166–176.
- Takaya, K., & Nakamura, H. (2013). Interannual variability of the East Asian winter monsoon and related modulations of the planetary waves. *Journal of Climate*, 26(23), 9445–9461.
- Thompson, D. W. J., & Wallace, J. M. (2001). Regional climate impacts of the Northern Hemisphere annular mode. *Science*, 293(5527), 85–89.
- Wang, B., Ho, L., Zhang, Y., & Lu, M. M. (2004). Definition of South China Sea monsoon onset and commencement of the East Asia summer monsoon. *Journal of Climate*, 17, 699–710.
- Wang, B., Wu, R. G., & Fu, X. H. (2000). Pacific-East Asian teleconnection: How does ENSO affect East Asian climate? *Journal of Climate*, 13(9), 1517–1536.
- Wang, H. (2001). The weakening of Asian monsoon circulation after the end of 1970s. *Advances in Atmospheric Sciences*, 18, 376–386.
- Wang, L., Chen, W., & Huang, R. (2008). Interdecadal modulation of PDO on the impact of ENSO on the East Asian winter monsoon. *Geophysical Research Letters*, 35, L20702. <https://doi.org/10.1029/2008GL035287>
- Wang, L., Chen, W., Zhou, W., & Huang, R. H. (2009). Interannual variations of East Asian trough axis at 500 hPa and its association with the East Asian winter monsoon pathway. *Journal of Climate*, 22(3), 600–614.
- Wu, B., & Wang, J. (2002). Winter Arctic Oscillation, Siberian High and East Asian winter monsoon. *Geophysical Research Letters*, 29(19), 1897. <https://doi.org/10.1029/2002GL015373>
- Wu, B., Zhou, T., & Li, T. (2009). Seasonally evolving dominant interannual variability modes of East Asian climate. *Journal of Climate*, 22, 2992–3005.
- Wu, Z., Li, J., Jiang, Z., & He, J. (2011). Predictable climate dynamics of abnormal East Asian winter monsoon: Once-in-a-century snowstorms in 2007/2008 winter. *Climate Dynamics*, 37, 1661–1669. <https://doi.org/10.1007/s00382-0010-00938-00384>
- Xie, S.-P., Hu, K., Hafner, J., Tokinaga, H., Du, Y., Huang, G., & Sampe, T. (2009). Indian Ocean capacitor effect on Indo-Western Pacific climate during the summer following El Niño. *Journal of Climate*, 22, 730–747.
- Xu, M., Chang, C.-P., Fu, C., Qi, Y., Robock, A., Robinson, D., & Zhang, H. (2006). Steady decline of east Asian monsoon winds, 1969–2000: Evidence from direct ground measurements of wind speed. *Journal of Geophysical Research*, 111, D24111. <https://doi.org/10.1029/2006JD007337>
- Xu, X. M., Trumbore, S. E., Zheng, S. H., Southon, J. R., McDuffee, K. E., Lutgen, M., & Liu, J. C. (2007). Modifying a sealed tube zinc reduction method for preparation of AMS graphite targets: Reducing background and attaining high precision. *Nuclear Instruments and Methods in Physics Research Section B: Beam Interactions with Materials and Atoms*, 259(1), 320–329.
- Yihui, D., & Chan, J. C. L. (2005). The East Asian summer monsoon: An overview. *Meteorology and Atmospheric Physics*, 89, 117–142.
- Yin, J.-J., Yuan, D. X., Li, H. C., Cheng, H., Li, T. Y., Edwards, R. L., et al. (2014). Variation in the Asian monsoon intensity and dry-wet conditions since the Little Ice Age in central China revealed by an aragonite stalagmite. *Climate of the Past*, 10(5), 1803–1816. <https://doi.org/10.5194/cp-10-1803-2014>
- Yu, R., Wang, B., & Zhou, T. (2004). Tropospheric cooling and summer monsoon weakening trend over East Asia. *Geophysical Research Letters*, 31, L22212. <https://doi.org/10.1029/2004GL021270>
- Zhang, R., Sumi, A., & Kimoto, M. (1996). Impact of El Niño on the East Asian monsoon: A diagnostic study of the '86/87 and '91/92 events. *Journal of the Meteorological Society of Japan. Ser. II*, 74, 49–62.
- Zhang, Y., Sperber, K. R., & Boyle, J. S. (1997). Climatology and interannual variation of the East Asian winter monsoon: Results from the 1979–95 NCEP/NCAR reanalysis. *Monthly Weather Review*, 125(10), 2605–2619.
- Zhao, S., Feng, T., Tie, X., Long, X., Li, G., Cao, J., et al. (2018). Impact of climate change on Siberian High and wintertime air pollution in China in past two decades. *Earth's Future*, 6, 118–1333.